Pressure control using stochastic cell rescaling

Pressure control using stochastic cell rescaling

Mattia Bernetti[1] and Giovanni Bussi[1, a)]
Scuola Internazionale Superiore di Studi Avanzati, Via Bonomea 265, Trieste 34136, Italy

(Dated: 15 January 2025)

Molecular dynamics simulations require barostats to be performed at constant pressure. The usual recipe is to employ the Berendsen barostat first, which displays a first-order volume relaxation efficient in equilibration but results in incorrect volume fluctuations, followed by a second order or Monte Carlo barostat for production runs. In this paper, we introduce stochastic cell rescaling, a first-order barostat that samples the correct volume fluctuations by including a suitable noise term. The algorithm is shown to report volume fluctuations compatible with the isobaric ensemble and its anisotropic variant is tested on a membrane simulation. Stochastic cell rescaling can be straightforwardly implemented in existing codes and can be used effectively both in equilibration and in production phases.

I. INTRODUCTION

Molecular dynamics (MD) simulations can be used to characterize the dynamical properties of microscopic systems by simulating their evolution according to the Hamilton equations of motion.[1] However, the Hamilton equations are valid only for isolated systems and need to be amended to describe the coupling with external baths. Most common cases are thermostats and barostats. The former are used to transfer heat so as to properly control temperature. The latter are used to transfer mechanical work, thereby allowing for external pressure, stress, or surface tension to be controlled. Pressure control in MD was first introduced in the pioneering work of Andersen[2] using an extended Lagrangian formalism. This framework was then extended to allow periodic cells of arbitrary shapes.[3,4] A number of variants of these methods have been published[5–17] with either improved integration schemes, small modifications to control errors when the number of simulated particles is small, or generalization to liquid interfaces. The volume degree of freedom can also be coupled to a stochastic thermostat in a so-called Langevin piston approach.[18–24] All the methods mentioned so far associate an inertia to the volume, resulting in a second-order differential equation for its time evolution, which is stochastic for Langevin piston algorithms. An alternative approach is to use a Monte Carlo procedure to resample the volume every few steps of MD.[25,26] The Monte Carlo barostat is simpler to implement, since it does not require the calculation of the virial, but it is sometime considered less efficient than virial-based barostats.[27] The only barostat based on a first-order differential equation is the weak coupling or Berendsen barostat.[28] This barostat intuitively changes the volume by an increment proportional to the difference between the internal and external pressure and is very efficient in equilibrating the system. However, it does not sample a predictable ensemble. The usual rule of the thumb is thus to use the Berendsen barostat for equilibration, followed by either a second-order barostat or a Monte Carlo barostat for production (see Fig. 1, middle panel).[29]

In this work, we propose a new scheme that is based on a first-order differential equation but, at variance with the Berendsen scheme, samples the correct isothermal-isobaric ensemble (see Fig. 1, lower panel). To achieve this result, we add a suitably designed stochastic term to the Berendsen barostat, in the spirit of what was done in the stochastic velocity rescaling algorithm[30] to amend the Berendsen thermostat. The resulting algorithm can also be seen as a high-friction variant of the Langevin piston barostat. We derive and test several possible integration schemes and provide a reference implementation for all of them in an educational MD code. One of the integration schemes is also implemented and tested in a modified version of the popular MD code GROMACS.[31] The algorithm produces correct volume fluctuations for a wide range of the control parameters in a Lennard-Jones fluid and

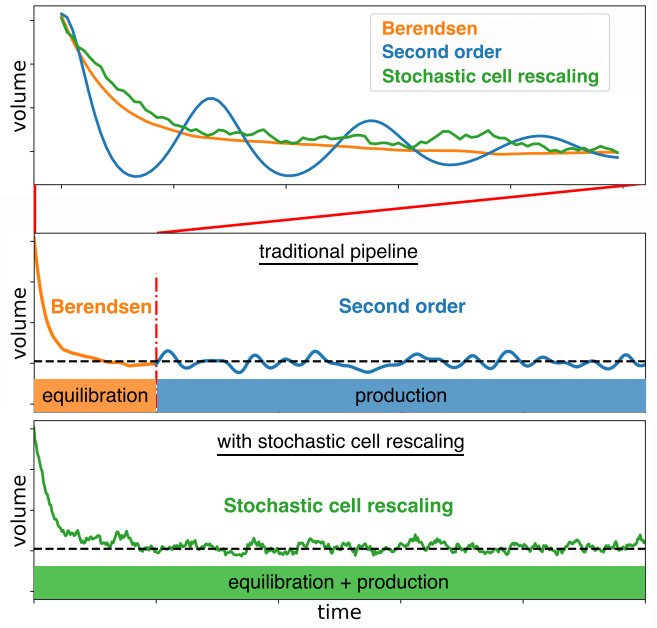

FIG. 1. Graphical representation of protocols for a constant-pressure simulation. In the traditional pipeline (middle panel), an equilibration run using a first-order Berendsen barostat[28] is followed by a production run using a second-order barostat.[2–24] Indeed, using a second-order barostat on a non-equilibrated system might lead to oscillations and instabilities (upper panel). The here introduced stochastic cell rescaling algorithm relaxes straight to the correct volume and then produces correct fluctuations (lower panel). It can thus be used both for equilibration and production runs.

a)Electronic mail: bussi@sissa.it

in liquid water. The method is also tested on the calculation of solvation free energies, for which a recent paper suggested incorrect results arising from use of the Berendsen barostat,[32] and its semi-isotropic version is tested on a membrane simulation.

II. METHODS

A. Stochastic cell rescaling

We consider a system composed of N atoms with coordinates and momenta $\boldsymbol{q}_i$ and $\boldsymbol{p}_i$ contained in a box of volume V. For compactness, in the following we indicate the vector of all coordinates and momenta as q and p, respectively. According to Hamilton equations, p and q evolve as

$$d\boldsymbol{p}_i = -\frac{\partial U}{\partial \boldsymbol{q}_i} dt \tag{1a}$$

$$d\boldsymbol{q}_i = \frac{\boldsymbol{p}_i}{m_i} dt \tag{1b}$$

where t is the time, m_i is the mass of the i-th particle, and U the potential energy of the system, which depends on the positions q.

To obtain ensemble averages in the NPT ensemble, where the number of particles, the external pressure, and the temperature are constant, the volume V has to be allowed to fluctuate so as to sample states with probability

$$\mathscr{P}(p,q,V) \propto e^{-\frac{K+U+P_0V}{k_BT}} . \tag{2}$$

Here, $K = \sum_i p_i^2/(2m_i)$ is the kinetic energy of the system, P_0 is the external pressure, k_B is the Boltzmann constant and T is the temperature. Equation 2 can be equivalently written as

$$-k_BT \log \mathscr{P}(p,q,V) = K + U + P_0V + C \tag{3}$$

where C is an arbitrary constant.

The goal of a barostat is to induce changes in the volume V that preserve the NPT distribution. These changes are typically made at constant scaled positions $s = q/\sqrt[3]{V}$, so that Cartesian positions q have to be uniformly scaled. Many algorithms implement this change at constant scaled momenta $\pi = p\sqrt[3]{V}$ as well, thus scaling Cartesian positions q and momenta p with inverse factors.[2–7,11–14,16,18,19,22,23] This scaling preserves the phase-space volume and originally stems from the use of a Hamiltonian formalism in the Andersen barostat.[2] In other methods, this scaling factor is modified by a small correction that vanishes as the number of atoms in the simulated box grows.[8–10,15,17,20,24] However, provided one evaluates the compression factor properly, scaling momenta is not strictly necessary, as suggested in Ref. 21. In the derivation below, we will assume that momenta are scaled with an inverse factor with respect to positions. A similar algorithm can be derived assuming that momenta are not scaled (see Sec. II B).

To obtain a continuous trajectory, we consider changes of V obtained by the solution of a first-order differential equation. The most general first-order differential equation for the single variable V with a preassigned stationary distribution $\mathscr{P}(V)$ is stochastic and has the following form:

$$dV = D\frac{\partial \log(D\mathscr{P})}{\partial V} dt + \sqrt{2D} dW . \tag{4}$$

Here dW is a Wiener noise and the equation is written using Ito stochastic calculus.[33] D is an arbitrary function of the volume V that can be interpreted as a diffusion coefficient. The stationarity of distribution $\mathscr{P}$ can be demonstrated by considering the associated Fokker-Planck equation $\frac{\partial \mathscr{P}}{\partial t} = -\frac{\partial}{\partial V}\left(D\mathscr{P}\frac{\partial \log D\mathscr{P}}{\partial V} - \frac{1}{2}\frac{\partial}{\partial V}(2D\mathscr{P})\right) = 0$. By inserting Eq. 3 in Eq. 4, with simple manipulation, the most general stochastic differential equation for V preserving the isothermal-isobaric distribution can be shown to be in the form

$$dV = -\frac{D}{k_BT}\left(\frac{\partial K}{\partial V} + \frac{\partial U}{\partial V} + P_0 - \frac{k_BT}{D}\frac{\partial D}{\partial V}\right) dt + \sqrt{2D} dW .$$

We notice that the term $\frac{\partial U}{\partial V}$ is meant to be taken at fixed scaled coordinates and corresponds to the negative of the contribution of the potential energy to the internal pressure. The term $\frac{\partial K}{\partial V}$ instead has to be computed at fixed scaled momenta, thus defining $K = V^{-2/3}\sum_i \pi_i^2/(2m_i)$. We thus have $\frac{\partial K}{\partial V} = -\frac{2K}{3V}$, and this term corresponds to the negative of the kinetic contribution to the internal pressure. The center-of-mass contribution to the internal pressure might be optionally included (see Supplementary Material, Sec. I).

We then arbitrarily set $D = \frac{\beta_T V k_B T}{\tau_P}$, where β_T is an estimate of the isothermal compressibility of the system and τ_P is a characteristic time associated to the barostat. The resulting differential equation is

$$dV = -\frac{\beta_T V}{\tau_P}\left(\frac{\partial K}{\partial V} + \frac{\partial U}{\partial V} + P_0 - \frac{k_BT}{V}\right) dt + \sqrt{\frac{2k_BT\beta_T V}{\tau_P}} dW .$$

This equation on V can be converted to an equivalent equation on the strain $\varepsilon = \log(V/V_0)$, where V_0 is a reference volume that is needed to have the correct dimensionality,[34] and can be arbitrarily set to $V_0 = 1\text{nm}^3$. By means of the Ito chain rule,[33] one obtains

$$d\varepsilon = -\frac{\beta_T}{\tau_P}(P_0 - P_{\text{int}})\, dt + \sqrt{\frac{2k_BT\beta_T}{V\tau_P}} dW , \tag{5}$$

where $P_{\text{int}} = \frac{2K}{3V} - \frac{\partial U}{\partial V}$ might be computed either including or excluding the center-of-mass contribution (see Supplementary Material, Sec. I). The interpretation of Eq. 5 is straighforward. The deterministic term increases or decreases the volume when the internal pressure is respectively larger or smaller than the external one. Thanks to our definition of D, this term is equivalent to the one used in the popular Berendsen barostat.[28] The stochastic term, however, allows volume fluctuations to be properly controlled. Equation 5 can be also derived by taking the high-friction limit of a Langevin piston algorithm[14,18] with a volume-dependent friction, provided the additional drift is taken into account correctly[35] (see Supplementary Material, Sec. II). Equation 5 can then be coupled

with Hamilton equations 1a and 1b and with a thermostat to sample the isothermal-isobaric ensemble. The increment in the volume logarithm leads to a rescaling of the cell matrix. We thus refer to this scheme as stochastic cell rescaling.

B. Working with unscaled momenta

The derivation reported in the previous Section assumes that volume changes are operated at constant scaled positions s and momenta π. It is possible to keep scaled positions s and physical momenta p fixed, instead, resulting in an algorithm where momenta are not scaled when volume changes. In this case, an extra factor V^N has to be inserted in Eq. 2, that in turn results in the use of the external temperature in evaluating the ideal gas pressure contribution in P_{int}. At the same time, the gradient of the kinetic energy with respect to the volume used in Eq. 4 would be zero. It can be seen that this change simply leads to the need to compute the internal pressure using the average kinetic energy instead of the instantaneous one.[21]

In brief, two formulations of our algorithm are possible:

- A formulation where momenta are scaled by a factor that is the inverse of the factor used to scale the positions, and the internal pressure is calculated as $P_{\text{int}} = \frac{2K}{3V} - \frac{\partial U}{\partial V}$.
- A formulation where momenta are untouched while scaling the simulation box, and the internal pressure is calculated as $P_{\text{int}} = \frac{Nk_BT}{V} - \frac{\partial U}{\partial V}$.

If using a global thermostat so that center-of-mass momentum is conserved, N should be replaced with $N-1$. See Supplementary Material, Sec. I, for further discussion on the center-of-mass contribution to the internal pressure.

We notice that most barostat implementations choose the first formulation, which makes deriving a reversible integrator slightly more complex since positions and momenta must be evolved simultaneously. However, this formulation might be convenient when using constraints[36,37] or rigid bodies.[38] In these cases, indeed, the probability distributions of positions and momenta do not factorize, making the ideal gas contribution more difficult to compute, whereas the kinetic tensor implicitly contains the information about the position-dependent distribution of momenta. Ref. 21 uses the second formulation instead. Also the Monte Carlo barostat described in Refs. 25 and 26 does not scale momenta, and indeed includes explicitly a $(V'/V)^N$ term in the acceptance calculation, where V' is the proposed volume. The Berendsen barostat[28] uses a hybrid formulation where the pressure is computed using the instantaneous kinetic energy, as in the first formulation, but the momenta are not scaled when changing the simulation volume, as in the second formulation.

The use of the instantaneous kinetic energy instead of its average value can be seen as a source of noise in the dynamics of the volume. In particular, the kinetic energy has fluctuations equal to $\sqrt{\frac{3N}{2}}k_BT$ and an autocorrelation time τ_K that is system dependent and that can be controlled by choosing the parameters of the thermostat. These fluctuations can be approximated as an additional noise term in Eq. 5. If τ_K is significantly smaller than the relaxation time of the volume ($\tau_K \ll \tau_P$) this noise can be considered as white and equal to $\frac{\beta_T}{\tau_P}\frac{2}{3V}\sqrt{\frac{3N}{2}}k_BT\sqrt{\tau_K}dW = \frac{\beta_T k_BT}{\tau_P V}\sqrt{\frac{2N\tau_K}{3}}dW$. The ratio between the standard deviation of this noise and the standard deviation of the random noise in Eq. 5 is

$$\frac{\frac{\beta_T k_BT}{\tau_P V}\sqrt{\frac{2N\tau_K}{3}}}{\sqrt{\frac{2k_BT\beta_T}{V\tau_P}}} = \sqrt{\frac{\tau_K N k_BT\beta_T}{3\tau_P V}} \approx \sqrt{\frac{\tau_K N\sigma_V^2}{3\tau_P\langle V\rangle^2}}\,. \qquad (6)$$

In the last step we exploited the fact that $\beta_T = \frac{\sigma_V^2}{\langle V\rangle k_BT}$, where σ_V^2 are the fluctuations of the volume, and we approximated V with its average value $\langle V\rangle$. Since in condensed phases we expect the relative volume fluctuations to be smaller than $\sqrt{1/N}$, and we assumed $\tau_K \ll \tau_P$, the contribution of the additional noise is negligible. This is the case for most of the practical applications considered here, with the used thermostat settings. However, in general settings, the two sources of noise might be comparable. It is thus important to implement stochastic cell rescaling so that, if the internal pressure is computed using the instantanous kinetic energy, momenta are scaled with the correct factor whenever the volume changes.

C. Effective energy drift

Stochastic cell rescaling is based on the use of Hamilton equations 1a and 1b and of the stochastic differential equation 5, both satisfying detailed balance. When they are integrated with a finite time step algorithm, however, detailed balance is violated. This violation can be monitored during the simulation[30,39] and used to determine if the time step and the other simulation parameters were chosen correctly, to verify that forces are correctly computed as the negative derivatives of the energy function, or to compute the acceptance for a so-called Metropolized integrator.[40] This contribution can be interpreted as the work performed by the integration algorithm on the system.[41] In the case of pure Hamilton equations, this drift corresponds exactly to the change in the total energy of the system. When a thermostat is used, its contribution to the drift has to be added.[30,39] Similarly, the barostat will contribute to the drift.

In order to compute the contribution of the barostat to the drift, it is necessary to compute the relative probabilities of generating forward steps, where $\varepsilon \to \varepsilon'$, and backward steps, where $\varepsilon' \to \varepsilon$. We notice that the prefactor of the stochastic term in Eq. 5 depends explicitly on ε. As discussed in more details in Supplementary Material, Sec. III, this dependence might increase detailed-balance violations. By performing a change of variable to $\lambda = e^{\varepsilon/2}\sqrt{V_0} = \sqrt{V}$, instead, by means of the Ito chain rule,[33] one obtains the following differential equation

$$d\lambda = -\frac{\beta_T\lambda}{2\tau_P}\left(P_0 - P_{\text{int}} - \frac{k_BT}{2V}\right)dt + \sqrt{\frac{k_BT\beta_T}{2\tau_P}}dW\,. \qquad (7)$$

In this equation, the prefactor of the stochastic term is a constant. By simply integrating this equation with finite difference increments, the drift can be computed in the same way as it is computed in the high-friction limit of the Langevin equation,[39] and corresponds to the calculation of the acceptance in the so-called smart Monte Carlo method[42] (see Supplementary Material, Sec. IV).

It it important to recall that the effective energy drift quantifies how much detailed balance is violated. However, detailed balance is not a necessary condition for reaching the target stationary distribution.[43] In addition, it has been shown that this drift might overestimate the errors observed in sampling the configurational degrees of freedom.[44]

D. Integration of the equations of motion

We considered three different ways to integrate Eqs. 1a, 1b, and 5. In all of them, it is possible to postpone the calculation of the virial to every N_P steps in a multiple-time-step fashion[45] in order to speed up the calculation. In the last two algorithms, it is possible to define the effective energy drift (see Sec. II C). More details are reported in Supplementary Material, Sec. V.

Euler integrator. The volume is evolved by propagating its logarithm using a finite time step approximation of Eq. 5. Positions and velocities are then evolved using velocity Verlet. Forces *are not* recomputed after the volume change. As a consequence, the obtained trajectory *is not* reversible.

Reversible Euler integrator. The volume is evolved by propagating its square root using a finite time step approximation of Eq. 7. Positions and velocities are then evolved using velocity Verlet. Forces *are* recomputed after the volume change. As a consequence, the obtained trajectory *is* reversible. However, this is paid with an extra force calculation every N_P steps. In order to quantify the effective energy drift, the virial needs to be recomputed after the volume change.

Trotter-based integrator. The volume is evolved by propagating its square root using a finite time step approximation of Eq. 7. Positions and velocities are evolved using velocity Verlet simultaneously with volume change using a Trotter splitting. There is no need to recompute forces after the volume change. However, in order to quantify the effective energy drift, the virial needs to be computed also at the step immediately after the one at which scaling was applied. The obtained trajectory *is* reversible.

For simplicity, we decided to use Eq. 5 in the Euler integrator, where the effective energy drift would not be well-defined anyway, whereas we used Eq. 7 for the reversible implementations. All the three schemes can be implemented either scaling or not scaling velocities upon volume change (see Sec. II B). For each of the integrators, Table I summarizes the cost in term of how many force and virial calculations are required on average for each simulation step. These integrators, similarly to those discussed in Ref. 17, can in principle be used with an arbitrarily large N_P, provided that τ_P is also chosen large enough.

Integrator	Reversible	N_{forces}	N_{virial}
Euler	no	1	$1/N_P$
Reversible Euler	yes	$1+1/N_P$	$2/N_P$
Trotter	yes	1	$\min(1,2/N_P)$

TABLE I. Computational overhead for the discussed integrators. Integrators are named as discussed in the main text. N_P is stride for the propagation of the barostat. N_{forces} and N_{virial} are the average number of times forces and virial need to be calculated for every MD step, respectively. For all the integrators, the equation of the barostat is propagated every $1/N_P$ steps.

E. Semi-isotropic version

Eq. 5 can be generalized to cases where ε is a matrix representing the deformation of the system. We here derive the equations required to sample the constant surface-tension ensemble $NP\gamma T$, where the equilibrium probability reads[9]

$$\mathscr{P}(p,q,A,L) \propto e^{-\frac{K+U+P_0AL-\gamma_0 A}{k_BT}} . \tag{8}$$

Here A is the area of the simulation box in the xy plane, L is its height, and γ_0 is the surface tension multiplied by the number of surfaces.

We arbitrarily set the diffusion coefficients for A and L as $D_A = \frac{2\beta_T A^2 k_B T}{3V\tau_P}$ and $D_L = \frac{\beta_T L^2 k_B T}{3V\tau_P}$, respectively. By defining the variables $\varepsilon_{xy} = \log(A/A_0)$ and $\varepsilon_z = \log(L/L_0)$, and following a procedure similar to the one above, these equations of motion are obtained:

$$d\varepsilon_{xy} = -\frac{2\beta_T}{3\tau_P}\left(P_0 - \frac{\gamma_0}{L} - \frac{P_{\text{int},xx}+P_{\text{int},yy}}{2}\right)dt + \sqrt{\frac{4k_BT\beta_T}{3V\tau_P}}dW_{xy} \tag{9a}$$

$$d\varepsilon_z = -\frac{\beta_T}{3\tau_P}(P_0 - P_{\text{int},zz})\,dt + \sqrt{\frac{2k_BT\beta_T}{3V\tau_P}}dW_z \tag{9b}$$

Here $P_{\text{int},xx}$, $P_{\text{int},yy}$, and $P_{\text{int},zz}$ are components of the internal pressure tensor and the two noise terms dW_{xy} and dW_z are explicitly written with different subscripts to remark that they have to be drawn independently. For an extensive derivation of Eqs. 9 see Supplementary Material, Sec. VI.

By taking the sum of the two equations above and setting $\gamma_0 = 0$, one obtains Eq. 5. This means that, if no external tension is applied, the dynamics of the volume in the semi-isotropic case will be identical to the isotropic case. In principle, it is possible to tune separately the compressibility of the system in the xy and z directions (see Supplementary Material, Sec. VII, for the special case where cell height L is kept constant), or even to choose a non-diagonal diffusion matrix for the A and L variables. This choice would only affect the timescale at which A and L equilibrate, leaving the sampled distribution unchanged.

F. Computational details

Simulations of the Lennard-Jones fluid were performed using a modified version of the SimpleMD program. A system

of $N = 256$ particles was simulated in a cubic box with a time step of 0.005 for 10^7 steps, accumulating statistics every 10 steps. Forces were truncated at distance 2.5. Temperature was set to $T = 1.5$ and controlled with a stochastic velocity rescaling thermostat[30] with relaxation time $\tau_T = 0.05$. Pressure was set to $P_0 = 1$ and controlled using stochastic cell rescaling with a range of control parameters. All parameters are reported in reduced Lennard-Jones units. All the reported quantities were computed discarding the initial 2.5×10^6 steps.

Simulations of the liquid water, host-guest and guest only, and the membrane systems were performed with a modified version of GROMACS 2019.4.[31] The liquid water system comprised 2850 waters in a rhombic dodecahedron box. The TIP3P model[46] was used to represent the water molecules. A short equilibration run lasting 500 ps was first conducted in the *NVT* ensemble. The production phase consisted of three sets of *NPT* simulations using the Parrinello-Rahman,[4] Berendsen,[28] and stochastic cell rescaling barostats, respectively. In each set, a range of control parameters was explored, using 1 bar as reference for isotropic pressure coupling in all cases. All simulations lasted 10 ns and statistics were saved every 200 steps (0.4 ps). The reference temperature was 300 K in all runs and was controlled through a stochastic velocity rescaling thermostat[30] with a relaxation time $\tau_T = 0.1$ ps. A Verlet cut-off scheme was employed for neighbor searching, updating the neighbor list every 10 steps. All shown results were obtained discarding the first 2 ns of simulation.

A smaller water box, comprising 900 TIP3P water molecules, was employed to perform the physical validation tests indicated in Refs. 47 and 48. To conduct these tests, the physical_validation package, an open-source and platform-independent Python library (https://physical-validation.readthedocs.io) in which they are implemented, was used. For each barostat (Berendsen, Parrinello-Rahman and stochastic cell rescaling), two simulations of 10 ns each were run at the reference pressure of 1 bar and 301 bar, respectively, with $N_P = 10$ steps and $\tau_P = 1$ ps for Berendsen and Parrinello-Rahman and $\tau_P = 0.5$ ps for stochastic cell rescaling. All GROMACS input files were taken and adapted from the examples/water_ensemble subfolder coming with the package.

Free energy differences for the host-guest (OA-G3) and guest only (G3) systems were computed from expanded ensemble simulations in solution, conducted using coordinates, topology, and set-up provided by Ref. 32. A detailed description of the simulation parameters can be found therein. Briefly, decoupling of the guest was achieved by completely turning off charges first and then removing Van der Waals interactions in both the host-guest and guest only systems. The entire procedure comprised a total of 40 lambda windows. A velocity Verlet integrator was used with a time step of 2 fs. The expanded ensemble simulations were divided in two stages: an initial equilibration stage to adaptively estimate the expanded ensemble weights and the following production phase in which the weights were kept fixed. For the host-guest system, 60 ns were required for the equilibration of weights with Berendsen and stochastic cell rescaling, while for the guest only systems about 30 ns were necessary in all cases. From the production stage, free-energy differences were computed with the multistate Bennett acceptance ratio (MBAR) method[49] using the alchemical_analysis tool version 1.0.2[50] along with pymbar version 3.0.5. The free energy associated to the presence of the restraints on the center of mass in the decoupled state was computed as $\Delta G_{\text{restr}} = -\frac{3}{2}\log\left(\frac{2\pi k_B T}{k}\right) + \log V_{\text{mol}} = 16.73$ kJ/mol, where $k = 1000$ kJ/(mol·nm^2) is the coupling constant and $V_{\text{mol}} = 1.66$ nm^3 is the volume corresponding to the one molar standard state.

Replica exchange simulations for decoupling of the guest only in solution were performed using 40 replicas corresponding to the windows employed to turn off charges and removing Van der Waals interactions in the expanded ensemble simulations, thus resulting in a Hamiltonian replica-exchange protocol. Two variants of the system with varying size of the box were considered: the same used for the expanded ensemble simulations, taken from Ref. 32, where a distance of 1.2 nm from all guest heavy atoms in all directions was applied, and a smaller one where such distance was set to 0.8 nm. A leap-frog integrator was used with a time steps of 2 fs and exchanges between replicas were attempted every 400 steps (0.8 ps). Production runs were conducted for a total of 5 ns/replica and were used to compute the free-energy differences through Bennett's acceptance ratio method (BAR)[51] as implemented in the gmx bar module of GROMACS. Decoupling of the guest E20 (donepezil, extracted from PDB ID: 1EVE) was conducted according to the same set-up. Ligand parameters were determined using the General Amber Force Field (GAFF)[52] following the RESP procedure[53] to determine the molecule charges. During the simulations, the conformation of the ligand was kept fixed by restraining the root-mean-square displacement from the crystal conformation computed after superimposing the two structures. To this end, the RESTRAINT feature of the bias module of PLUMED[54] was used, setting a force constant of 209200 kJ/(mol·nm^2) for the harmonic restraint.

The membrane system was built as described in the "$KALP_{15}$ in DPPC" (the KALP model peptide in a lipid bilayer of dipalmitoylphosphatidylcholine) tutorial,[55] which protocol was based on a previous work[56] and used the GROMOS96 53A6 force field,[57] extended to include Berger lipid parameters.[58] The procedure included usage of the InflateGRO methodology[59] to pack the lipids around the embedded protein. After solvation, a system comprising 126 DPPC lipid and 4182 SPC water molecules[60] was obtained. Energy minimization and equilibration of the system were conducted as described in detail in the tutorial. As for the liquid-water system, the production phase consisted of three sets of *NPT* simulations using the Parrinello-Rahman, Berendsen and stochastic cell rescaling barostats. A reference pressure of 1 bar was employed for semi-isotropic pressure coupling in all cases, along with $\tau_P = 2$ ps and a compressibility of $4.5\text{x}10^{-5}$ bar^{-1}. The temperature was set to 323 K and was controlled through the Nose-Hoover thermostat[6,61] with a relaxation time $\tau_T = 0.5$ ps, coupling separately a first group comprising the protein and DPPC lipids and a second one including the solvent and ion molecules. All simulations lasted

100 ns and statistics were saved every 200 steps (0.4 ps). All shown results were obtained analyzing the second half of the trajectory.

In all simulations, statistical errors were determined using block analysis[62] with a variable number of blocks and conservatively using the largest estimate for the error. For all the simulations performed using the Parrinello-Rahman barostat, fluctuations were imposed to be isotropic (Lennard-Jones fluid, liquid water and guest-only systems) or semi-isotropic (membrane system), as implemented in GROMACS. Indeed, the fully flexible version of the Parrinello-Rahman barostat is known to be unstable in these cases. The resulting equations of motion for the box are thus not exactly equivalent to those of the Andersen[2] or Martyna-Tobias-Klein[8] algorithms, but are representative of a second-order barostat.

III. NUMERICAL TESTS

A. Lennard-Jones fluid

We tested stochastic cell rescaling on the simulation of a Lennard-Jones fluid in the NPT ensemble. We first performed a range of simulations at constant volume, computed the average internal pressure, and integrated it so as to obtain a reference distribution for the volume V. The predicted volume fluctuations correspond to an isothermal compressibility $\beta_T \approx 0.3$. This value is used as an input in the simulations performed with the barostat. The distribution of the volume obtained using barostat parameters $N_P = 1$ and $\tau_P = 1$ is perfectly overlapping with the reference one (see Fig. S1).

We then evaluated the robustness of the results by monitoring volume average and fluctuations when changing barostat parameters, testing the three discussed integrators (Fig. 2). We first fixed $N_P = 1$ and investigated the dependence of the results on τ_P (Fig. 2a). Any $\tau_P \geq 0.1$ report results consistent with the reference. As expected, the statistical error on the volume and on its fluctuations grows with τ_P. This suggests that, in order to equilibrate and sample the volume variable as quickly as possible, τ_P should be chosen as small as possible. The autocorrelation time of V can be seen to be close to τ_P when τ_P is large enough (see Fig. S2). The relationship between stochastic cell rescaling and the Langevin piston approach can be appreciated by comparing the autocorrelation function of the volume in a Langevin piston with decreasing values of the barostat mass (see Fig. S3). We then fixed $\tau_P = 1$ and investigated the dependence of the results on N_P (Fig. 2b). $N_P \geq 10$ resulted in a volume variance observably larger than its reference value. Interestingly, the three introduced integrators resulted in very similar accuracy when used with the same parameters.

For the two integrators that allow an effective energy drift to be defined, we computed this drift for all the chosen sets of parameters (Fig. 2c). As long as $\tau_P \geq 1$ and $N_P = 1$ the drift was of the order of 10^{-6} energy units per step, comparable to the one obtained in NVT simulations. By testing different values of N_P, we observed that the drift steadily grew with N_P. This drift can be used to estimate if the violations of detailed balance induced by the barostat are exceeding those that are present also in absence of the barostat.[14]

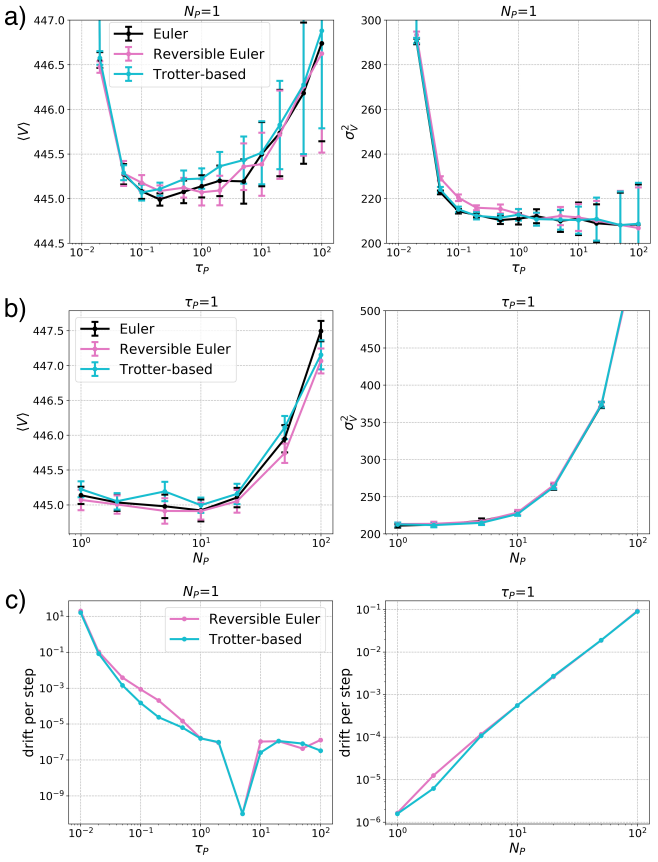

FIG. 2. Results from simulations of a Lennard-Jones fluid. a) Average and fluctuations of the volume (left and right panels, respectively) as a function of the time constant for pressure coupling (τ_P) at fixed frequency for pressure coupling ($N_P = 1$). b) Average and fluctuations of the volume (left and right panels, respectively) as a function of the frequency for pressure coupling (N_P) at fixed time constant for pressure coupling ($\tau_P = 1$). c) Effective energy drift per step, obtained from the slope of a line interpolating the effective energy drift on the entire trajectory. With some settings, a negative slope is obtained and is here shown as 10^{-10}.

All the reported results were obtained using the formulation in which momenta are scaled when volume changes (see Sec. II B). Results obtained without scaling momenta were equivalent and are reported in Fig. S4.

B. Liquid water

We then tested stochastic cell rescaling on the simulation of a box of TIP3P water molecules. These simulations were done using GROMACS, which includes an implementation of the Parrinello-Rahman algorithm[4] that is known to report results in the NPT ensemble and can thus be used as a reference. We also tested the Berendsen algorithm,[28] that neglects the noise term and is expected produce incorrect volume fluctuations. In the comparison between the Parrinello-Rahman

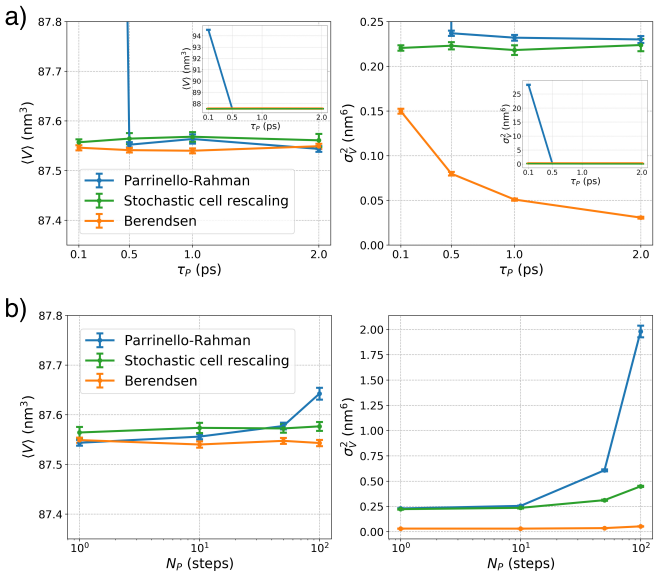

FIG. 3. Results from simulations of a TIP3P water box. a) Average and fluctuations of the volume (left and right panels, respectively) as a function of the time constant for pressure coupling (τ_P) at fixed frequency for pressure coupling ($N_P = 1$). b) Average and fluctuations of the volume (left and right panels, respectively) as a function of the frequency for pressure coupling (N_P) at fixed time constant for pressure coupling ($\tau_P = 2$ for Parrinello-Rahman and Berendsen, $\tau_P = 0.5$ for stochastic cell rescaling).

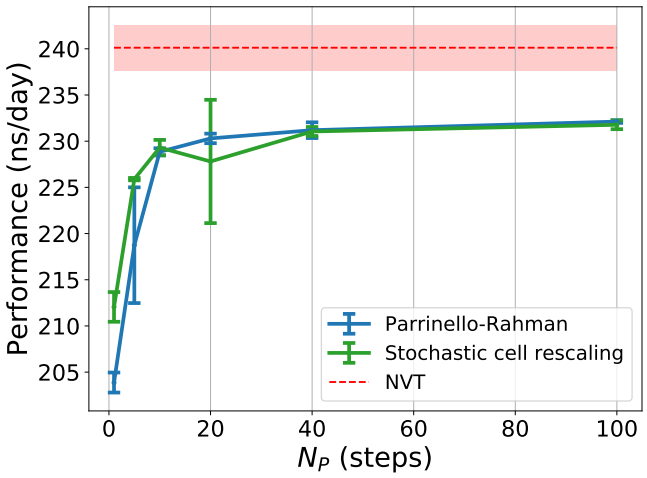

FIG. 4. Dependence of performance on choice of N_P. Results are for the water box simulation in GROMACS and were produced using 4 cores on a Intel® Xeon® CPU E5-2620 v2 (2.10GHz) and 1 NVIDIA GeForce GTX TITAN GPU. Error bars report the standard deviation over 5 simulations lasting 1 ns. The red dashed line and shade report the performance and standard deviation, respectively, of an NVT simulation for the same system.

and the two other schemes, one should consider that there is not an equivalence in the definition of τ_P. Thus, results at the same τ_P cannot be directed compared.

We first analyzed the dependence of volume averages and fluctuations as a function of τ_P, setting $N_P = 1$ (Fig. 3a). Volume averages were always consistent in the three schemes, but the Parrinello-Rahman implementation showed some instability for the smallest choice of $\tau_P = 0.1$ ps. Volume fluctuations obtained with Parrinello-Rahman and with stochastic cell rescaling were consistent and lead to an estimate of the isothermal compressibility equal to $\beta_T = \frac{\sigma_V^2}{\langle V \rangle k_B T} \approx 1.05 \times 10^{-3} \frac{\text{nm}^3}{\text{kJ/mol}} \approx 6.3 \times 10^{-5} \text{bar}^{-1}$. These results are consistent with those reported in Ref. 63 for the same water model. We notice that this value is markedly different from the experimental value $\beta_{T,\text{exp}} = 4.5 \times 10^{-5} \text{bar}^{-1}$. This discrepancy is known for the TIP3P model. The experimental compressibility has been here used as an input parameter. The effect of choosing an input compressibility that is inconsistent with the compressibility of the simulated system is only to change the effective relaxation time of the volume, as it can be seen by computing its autocorrelation function (see Fig. S5). Fluctuations were significantly underestimated by the Berendsen barostat. Counterintuitively, the fluctuations reported by the Berendsen barostat increased when τ_P decreased. We interpret this effect as a consequence of the fact that the amplitude of the fictitious noise that is implicitly included in the Berendsen barostat by the usage of the instantaneous kinetic energy grows when τ_P decreases (see Eq. 6), partly compensating for the lack of an explicit noise term.

We then analyzed the dependence of volume averages and fluctuations as a function of N_P, setting $\tau_P = 2$ ps for Parrinello-Rahman and Berendsen and $\tau_P = 0.5$ ps for stochastic cell rescaling (Fig. 3b). In all cases, a too large N_P resulted in an overestimation of the fluctuations. For this specific system and simulation parameters, $N_P = 10$ seems a reasonable compromise for all barostats. We notice that $N_P = 10$ is already capable to give a significant performance boost (see Fig. 4).

A validation similar to the one reported in Refs. 47 and 48 was then performed on a smaller water box. The results are reported in Fig. S6 and in Table S1, and confirm that the quality of the volume distributions obtained with our implementation of the stochastic cell rescaling algorithm is significantly more reliable than the one obtained with the Berendsen barostat. Interestingly, stochastic cell rescaling appears as slightly closer to the reference result than the Parrinello-Rahman barostat (Table S1), although this might depend on the technical details of the integration scheme implemented in GROMACS.

C. Free energy differences

We then tested the impact of the barostat algorithm on the calculation of the solvation and absolute binding free energies for small molecules. This is a relevant case since the incorrect volume fluctuations produced by the Berendsen barostat were recently suggested to significantly affect absolute binding affinities.[32] We here used the same settings reported in Ref. 32, and in particular the same extended ensemble protocol, on a host-guest system (OA-G3) and on a guest-only system (G3). Since the extended ensemble protocol is not com-

TABLE II. Free-energy differences (kJ/mol) for decoupling of the guest 5-hexenoic acid in host-guest (OA-G3) and guest only (G3) simulations in solution performed with the Expanded Ensemble method. ΔG in the standard state is computed subtracting the contribution of the restraint acting on the guest in the decoupled state.

	OA-G3	**G3**	ΔG
Berendsen	433.1 ± 0.6	389.0 ± 0.5	-27.3 ± 0.7
Stochastic cell rescaling	432.6 ± 0.6	387.9 ± 0.5	-28.0 ± 0.7

TABLE III. Free-energy of solvation (kJ/mol) computed from decoupling simulations of the guest (G3) and ligand E20 in solution performed with the Hamiltonian Replica Exchange method. The simulations of G3 were performed at varying box sizes: a larger one defined with a 1.2 nm distance (-d 1.2) from the guest in all directions, and a smaller one with a 0.8 nm distance (-d 0.8).

	G3 -d 1.2	**G3 -d 0.8**	**E20**
Berendsen	389.40 ± 0.05	389.65 ± 0.10	173.02 ± 0.14
Parrinello-Rahman	389.35 ± 0.17	389.03 ± 0.12	172.28 ± 0.13
Stochastic cell rescaling	389.41 ± 0.06	389.31 ± 0.14	172.70 ± 0.13

patible with the Parrinello-Rahman implementation present in GROMACS, we only report results obtained with stochastic cell rescaling and Berendsen algorithms. The solvation free energies obtained with different barostats are close to each other (see Table II). Their differences, which enter in the calculation of the absolute binding free energy, agree within the respective statistical error. We remark that the absolute binding free energies reported in Table II did not include corrections for finite size effects, and should not be compared quantitatively with those reported in Ref. 32. However, these corrections are expected to be independent of the choice of the barostat.

In order to better investigate the possible effects of incorrect volume fluctuations on the calculation of solvation free energies, we tested the guest-only system in a replica-exchange protocol that is compatible with the Parrinello-Rahman barostat implemented in GROMACS. In this case, the size of the water box was decreased so as to amplify the impact of the barostat algorithm (see Table III). For all the tested settings, the discrepancy between the results obtained with the Berendsen, stochastic cell rescaling, and Parrinello-Rahman barostats were below a fraction of kJ/mol. We notice that the reported estimate of the statistical error is likely an underestimation since it does not take into account the exchange of coordinates between the replicas. Tests performed with a larger ligand (E20), representative of typical drug molecules pursued in medicinal chemistry frameworks, confirm that differences are small ($<$ 1 kJ/mol) and likely not correlated or weakly correlated with the choice of the barostat.

D. Membrane simulation

We finally tested the impact of the barostat algorithm on the equilibration of a model membrane, including a short transmembrane protein. In this case we employed the anisotropic version of the stochastic cell rescaling, Berendsen, and Parrinello-Rahman algorithms, where no external tension is applied to the membrane. Whereas the simulations are probably too short to properly equilibrate this system, it is clear that stochastic cell rescaling and Parrinello-Rahman provide consistent results, whereas the Berendsen barostat leads to a suppression of the fluctuations both in the membrane surface and in the cell size in the direction orthogonal to the membrane (Table IV). Time series for the simulated trajectories are reported in Fig. S7.

IV. DISCUSSIONS

In this work, we introduced a barostat named stochastic cell rescaling that is driven by a first order differential equation on the volume. The formulation makes it very similar to the popular Berendsen barostat,[28] but includes a noise term to enforce the correct volume fluctuations. Being based on a first-order differential equation, the method can be used effectively in equilibration phases. The tested systems range from simple fluids to macromolecular constructs and are modeled using intra and inter-molecular interactions as well as constraints. A version suitable to control surface tension is also presented and tested on a membrane system. In all tested cases, the fluctuations obtained with a reference implementation of the Parrinello-Rahman algorithm were reproduced for a broad range of choices of the relaxation time of the barostat. Our algorithm can be implemented using either the instantaneous kinetic energy or its average value, resulting in very similar behaviors in the tested cases. The choice between the two formulations can be guided by practical reasons, such as the ease of their implementation in a given MD code. The algorithm can be easily modified to make usage of the molecular virial (see, *e.g.*, Refs. 12, 13, 17, and 22) provided that molecular positions and, optionally, velocities are scaled instead of atomic ones. Stochastic cell rescaling can in principle be combined with any thermostat to sample the isothermal-isobaric ensemble. In particular, in the membrane simulation presented here we tested its usage in combination with the Nose-Hoover thermostat,[6,61] whereas in the other simulations we used stochastic velocity rescaling.[30] In general, our recommendation would be Langevin dynamics,[64] if a local thermostat is desired to independently thermalize all degrees of freedom, or stochastic velocity rescaling, if a global thermostat is preferred so as to avoid slowing down particle diffusion.[65]

Similarly to the Berendsen barostat, our scheme has a single control parameter, τ_P, that controls the equilibration rate, but has to be complemented with an estimate of the isothermal compressibility of the system β_T. For the simulation of solvated systems, this compressibility is largely dependent on the properties of the solvent, so that in typical applications one can just use an estimate of its value for water. For other systems, it can be estimated by computing volume fluctuations σ_V in a test run and using the relationship $\beta_T = \frac{\sigma_V^2}{\langle V \rangle k_B T}$. In any case, only the ratio β_T/τ_P between these two parameters enters the algorithm, implying that an incorrect estimate of β_T by, for instance, a factor two would result in an error in the

TABLE IV. Average ($\langle V \rangle$) and fluctuations (var(V)) of the volume, area of the simulation box along the xy plane (A) and length of the box along the z axis (L) for a lipid membrane system. The system comprises a bilayer made up of DPPC lipids and the short transmembrane protein $KALP_{15}$. Note that the membrane is oriented in such a way that the lipid bilayer lies on the xy plane and the normal of the bilayer is aligned with the box z axis.

	Parrinello-Rahman	**Stochastic cell rescaling**	**Berendsen**
$\langle V \rangle$ (nm^3)	280.30 ± 0.03	280.23 ± 0.02	280.25 ± 0.03
σ_V^2 (nm^6)	0.723 ± 0.005	0.728 ± 0.010	0.227 ± 0.004
$\langle A \rangle$ (nm^2)	38.03 ± 0.07	37.88 ± 0.09	38.45 ± 0.09
σ_A^2 (nm^4)	0.35 ± 0.02	0.379 ± 0.015	0.277 ± 0.012
$\langle L \rangle$ (nm)	7.372 ± 0.014	7.399 ± 0.018	7.290 ± 0.016
σ_L^2 (nm^2)	0.0125 ± 0.0007	0.0143 ± 0.0006	0.0094 ± 0.0004

control of the relaxation time of the barostat of a factor two. Given the robustness of the results as a function of τ_P, we consider this as a minor drawback. We notice that this holds also for the original Berendsen barostat.

The relationship between stochastic cell rescaling and the Berendsen barostat is very similar to the relationship between stochastic velocity rescaling and the Berendsen thermostat. Importantly, the probability distribution of the kinetic energy is known *a priori*, allowing the equations of the stochastic velocity rescaling thermostat to be solved exactly.[30] On the contrary, the probability distribution of the volume depends in a non trivial manner on the coordinates. As a consequence, the barostat equations must be integrated approximately with a finite time step algorithm, and results might be incorrect if the coupling parameter τ_P is chosen too small. We here tested a number of algorithms showing that, whereas only some of them allow detailed-balance violations to be quantified, all of them can be used in practical applications for reasonable choices of the input parameters. We make available all the algorithms in an educational MD code and the simplest one in the GROMACS code. Source codes and instructions can be found at `http://github.com/bussilab/crescale`.

Stochastic cell rescaling can be seen as a first-order version of the Langevin piston algorithm,[18] and indeed it can be obtained by choosing a piston inertia small enough and a friction coefficient correspondingly large (see Supplementary Material, Sec. II). The analogy between the Langevin piston and the Berendsen barostat was already pointed out in Ref. 18, although resulting in a first-order equation that was suggested to be difficult to implement. Since the original Langevin piston algorithm was based on the Andersen thermostat, where absolute changes of the volume are driven rather than relative ones, the first-order equation suggested in Ref. 18 differs from Eq. 5, and its deterministic part thus differs from the one used in the Berendsen barostat. The advantage of the present formulation is that it can be straightforwardly implemented in any code supporting the Berendsen barostat, whereas a standard Langevin piston implementation should be built on top of a second-order barostat. In addition, stochastic cell rescaling works by construction in the high-friction limit and it is thus expected to be always stable in equilibration phases, still retaining the correct fluctuations in production runs.

A number of papers have shown artifacts related to the use of the Berendsen thermostat, see, *e.g.*, Refs. 47, 48, 66–68, including broken reversibility and incorrect fluctuations. The artifacts on the reversibility are relatively small.[68,69] The largest issue is the underestimation of energy fluctuations, that has an effect on replica-exchange simulations where the incorrectly distributed energies are used to compute acceptance probabilities.[67] The Berendsen barostat, similarly, is known to result in incorrect volume fluctuations (see, *e.g.*, Refs. 47, 48, and 70), and thus should not be used to evaluate compressibilities. The incorrect volume fluctuations could also introduce significant artifacts in replica-exchange simulations where replicas are simulated at different pressure[71] or surface tension.[72] In these cases, a barostat reproducing correct volume fluctuations has to be considered as mandatory. We here tested the result of free-energy calculations required to estimate ligand affinities, that were recently reported to be dependent on barostating details and, in particular, to display measurable artifacts induced by the use of the Berendsen barostat.[32] According to our results, all the tested barostats, including the Berendsen one, were leading to equivalent results in this specific application. This suggests that the discrepancies observed in Ref. 32 might be a consequence of some other implementation detail, and that artifacts of the Berendsen barostat on the properties of solvated molecules that are not directly correlated with volume fluctuations might be small. Nevertheless, we recommend stochastic cell rescaling as a better alternative since, thanks to the additional noise, it is guaranteed to sample the correct distribution.

The semi-isotropic version of stochastic cell rescaling was tested on a membrane simulation. These tests are more qualitative, since it is difficult to obtain statistically converged results on this system within the simulated time scales. Further tests will be necessary to see if pathological behaviors appear when the fraction of one phase is much larger than the fraction of the other phase, or when the difference in compressibility between the two phases is larger. It will be important to verify how stochastic cell rescaling compares with Parrinello-Rahman[4] and anisotropic Martyna-Tobias-Klein[8] algorithms in these difficult cases. A more flexible formulation where all the elements of the cell matrix can be adjusted will be the subject of a later work.

In summary, stochastic cell rescaling provides a simple first-order barostat that can be equally used in equilibration and production runs and can be adopted as a drop-in replacement of the Berendsen barostat, with minimal implementation changes that allow the isothermal-isobaric fluctuations to be properly sampled.

V. SUPPLEMENTARY MATERIAL

Supplementary Material includes Supplementary Methods related to the center-of-mass contribution to the pressure, the relationship with Langevin piston algorithm, more details on the integration of equations of motion and on the calculation of the energy drift, and the full derivation of the semi-isotropic version of the barostat. Supplementary Material also includes Supplementary Results related to the validation of the volume distributions, autocorrelation functions of the volume, results obtained with the formulation of the barostat where the average kinetic energy is used to compute the internal pressure, physical validation tests on a water box, and time series for the membrane simulations.

ACKNOWLEDGMENTS

Massimiliano Bonomi, Carlo Camilloni, Michele Ceriotti, Paolo Raiteri, and Michael Shirts are acknowledged for reading the manuscript and providing useful suggestions.

DATA AVAILABILITY

The data that support the findings of this study are openly available at `http://doi.org/10.5281/zenodo.3921886`. Analysis scripts and modified software can be found at `https://github.com/bussilab/crescale`.

[1] D. Frenkel and B. Smit, *Understanding molecular simulation: from algorithms to applications* (Acedemic Press, San Diego, 2001).
[2] H. C. Andersen, "Molecular dynamics simulations at constant pressure and/or temperature," J. Chem. Phys. **72**, 2384–2393 (1980).
[3] M. Parrinello and A. Rahman, "Crystal structure and pair potentials: A molecular-dynamics study," Phys. Rev. Lett. **45**, 1196 (1980).
[4] M. Parrinello and A. Rahman, "Polymorphic transitions in single crystals: A new molecular dynamics method," J. Appl. Phys. **52**, 7182–7190 (1981).
[5] S. Nosé and M. L. Klein, "Constant pressure molecular dynamics for molecular systems," Mol. Phys. **50**, 1055–1076 (1983).
[6] W. G. Hoover, "Canonical dynamics: Equilibrium phase-space distributions," Phys. Rev. A **31**, 1695 (1985).
[7] S. Melchionna, G. Ciccotti, and B. Lee Holian, "Hoover NPT dynamics for systems varying in shape and size," Mol. Phys. **78**, 533–544 (1993).
[8] G. J. Martyna, D. J. Tobias, and M. L. Klein, "Constant pressure molecular dynamics algorithms," J. Chem. Phys. **101**, 4177–4189 (1994).
[9] Y. Zhang, S. E. Feller, B. R. Brooks, and R. W. Pastor, "Computer simulation of liquid/liquid interfaces. i. theory and application to octane/water," J. Chem. Phys. **103**, 10252–10266 (1995).
[10] G. J. Martyna, M. E. Tuckerman, D. J. Tobias, and M. L. Klein, "Explicit reversible integrators for extended systems dynamics," Mol. Phys. **87**, 1117–1157 (1996).
[11] J. B. Sturgeon and B. B. Laird, "Symplectic algorithm for constant-pressure molecular dynamics using a Nosé–Poincaré thermostat," J. Chem. Phys. **112**, 3474–3482 (2000).
[12] G. Kalibaeva, M. Ferrario, and G. Ciccotti, "Constant pressure-constant temperature molecular dynamics: a correct constrained NPT ensemble using the molecular virial," Mol. Phys. **101**, 765–778 (2003).
[13] V. Marry and G. Ciccotti, "Trotter derived algorithms for molecular dynamics with constraints: Velocity Verlet revisited," J. Comput. Phys. **222**, 428–440 (2007).
[14] G. Bussi, T. Zykova-Timan, and M. Parrinello, "Isothermal-isobaric molecular dynamics using stochastic velocity rescaling," J. Chem. Phys. **130**, 074101 (2009).
[15] T.-Q. Yu, J. Alejandre, R. López-Rendón, G. J. Martyna, and M. E. Tuckerman, "Measure-preserving integrators for molecular dynamics in the isothermal–isobaric ensemble derived from the liouville operator," Chem. Phys. **370**, 294–305 (2010).
[16] P. Raiteri, J. D. Gale, and G. Bussi, "Reactive force field simulation of proton diffusion in BaZrO3 using an empirical valence bond approach," J. Phys. Condens. Matter **23**, 334213 (2011).
[17] R. A. Lippert, C. Predescu, D. J. Ierardi, K. M. Mackenzie, M. P. Eastwood, R. O. Dror, and D. E. Shaw, "Accurate and efficient integration for molecular dynamics simulations at constant temperature and pressure," J. Chem. Phys. **139**, 164106 (2013).
[18] S. E. Feller, Y. Zhang, R. W. Pastor, and B. R. Brooks, "Constant pressure molecular dynamics simulation: the Langevin piston method," J. Chem. Phys. **103**, 4613–4621 (1995).
[19] A. Kolb and B. Dünweg, "Optimized constant pressure stochastic dynamics," J. Chem. Phys. **111**, 4453–4459 (1999).
[20] D. Quigley and M. I. J. Probert, "Langevin dynamics in constant pressure extended systems," J. Chem. Phys. **120**, 11432–11441 (2004).
[21] N. Grønbech-Jensen and O. Farago, "Constant pressure and temperature discrete-time Langevin molecular dynamics," J. Chem. Phys. **141**, 194108 (2014).
[22] M. Di Pierro, R. Elber, and B. Leimkuhler, "A stochastic algorithm for the isobaric–isothermal ensemble with Ewald summations for all long range forces," J. Chem. Theory Comput. **11**, 5624–5637 (2015).
[23] X. Gao, J. Fang, and H. Wang, "Sampling the isothermal-isobaric ensemble by Langevin dynamics," J. Chem. Phys. **144**, 124113 (2016).
[24] S. Cajahuaringa and A. Antonelli, "Stochastic sampling of the isothermal-isobaric ensemble: Phase diagram of crystalline solids from molecular dynamics simulation," J. Chem. Phys. **149**, 064114 (2018).
[25] K.-H. Chow and D. M. Ferguson, "Isothermal-isobaric molecular dynamics simulations with Monte Carlo volume sampling," Comput. Phys. Commun. **91**, 283–289 (1995).
[26] J. Åqvist, P. Wennerström, M. Nervall, S. Bjelic, and B. O. Brandsdal, "Molecular dynamics simulations of water and biomolecules with a Monte Carlo constant pressure algorithm," Chem. Phys. Lett. **384**, 288–294 (2004).
[27] M. Harger and P. Ren, "Virial-based Berendsen barostat on GPUs using AMOEBA in Tinker-OpenMM," Results Chem. **1**, 100004 (2019).
[28] H. J. C. Berendsen, J. P. M. Postma, W. F. van Gunsteren, A. DiNola, and J. R. Haak, "Molecular dynamics with coupling to an external bath," J. Chem. Phys. **81**, 3684–3690 (1984).
[29] E. Braun, J. Gilmer, H. B. Mayes, D. L. Mobley, J. I. Monroe, S. Prasad, and D. M. Zuckerman, "Best practices for foundations in molecular simulations [article v1. 0]," Living J. Comp. Mol. Sci. **1**, 5957 (2019).
[30] G. Bussi, D. Donadio, and M. Parrinello, "Canonical sampling through velocity rescaling," J. Chem. Phys. **126**, 014101 (2007).
[31] M. J. Abraham, T. Murtola, R. Schulz, S. Páll, J. C. Smith, B. Hess, and E. Lindahl, "GROMACS: High performance molecular simulations through multi-level parallelism from laptops to supercomputers," SoftwareX **1–2**, 19–25 (2015).
[32] A. Rizzi, T. Jensen, D. R. Slochower, M. Aldeghi, V. Gapsys, D. Ntekoumes, S. Bosisio, M. Papadourakis, N. M. Henriksen, B. L. De Groot, Z. Cournia, A. Dickson, J. Michel, M. K. Gilson, M. R. Shirts, D. L. Mobley, and J. D. Chodera, "The SAMPL6 sampling challenge: Assessing the reliability and efficiency of binding free energy calculations," J. Comput. Aided Mol. Des. **34**, 601–633 (2020).
[33] C. W. Gardiner, *Handbook of stochastic methods* (Springer Berlin, 2009).
[34] C. F. Matta, L. Massa, A. V. Gubskaya, and E. Knoll, "Can one take the logarithm or the sine of a dimensioned quantity or a unit? dimensional analysis involving transcendental functions," J. Chem. Educ. **88**, 67–70 (2011).
[35] S. Hottovy, A. McDaniel, G. Volpe, and J. Wehr, "The Smoluchowski-Kramers limit of stochastic differential equations with arbitrary state-dependent friction," Commun. Math. Phys **336**, 1259–1283 (2015).
[36] J.-P. Ryckaert, G. Ciccotti, and H. J. C. Berendsen, "Numerical integration of the cartesian equations of motion of a system with constraints: molecular dynamics of n-alkanes," J. Comput. Phys. **23**, 327–341 (1977).
[37] B. Hess, H. Bekker, H. J. C. Berendsen, and J. G. E. M. Fraaije, "LINCS: a linear constraint solver for molecular simulations," J. Comput. Chem. **18**, 1463–1472 (1997).

[38]S. Miyamoto and P. A. Kollman, "Settle: An analytical version of the SHAKE and RATTLE algorithm for rigid water models," J. Comput. Chem. **13**, 952–962 (1992).
[39]G. Bussi and M. Parrinello, "Accurate sampling using Langevin dynamics," Phys. Rev. E **75**, 056707 (2007).
[40]A. Scemama, T. Lelièvre, G. Stoltz, E. Cancès, and M. Caffarel, "An efficient sampling algorithm for variational Monte Carlo," J. Chem. Phys. **125**, 114105 (2006).
[41]D. A. Sivak, J. D. Chodera, and G. E. Crooks, "Using nonequilibrium fluctuation theorems to understand and correct errors in equilibrium and nonequilibrium simulations of discrete Langevin dynamics," Phys. Rev. X **3**, 011007 (2013).
[42]P. J. Rossky, J. D. Doll, and H. L. Friedman, "Brownian dynamics as smart Monte Carlo simulation," J. Chem. Phys. **69**, 4628–4633 (1978).
[43]V. I. Manousiouthakis and M. W. Deem, "Strict detailed balance is unnecessary in Monte Carlo simulation," J. Chem. Phys. **110**, 2753–2756 (1999).
[44]J. Fass, D. A. Sivak, G. E. Crooks, K. A. Beauchamp, B. Leimkuhler, and J. D. Chodera, "Quantifying configuration-sampling error in Langevin simulations of complex molecular systems," Entropy **20**, 318 (2018).
[45]M. E. Tuckerman, G. J. Martyna, and B. J. Berne, "Molecular dynamics algorithm for condensed systems with multiple time scales," J. Chem. Phys. **93**, 1287–1291 (1990).
[46]W. L. Jorgensen, J. Chandrasekhar, J. D. Madura, R. W. Impey, and M. L. Klein, "Comparison of simple potential functions for simulating liquid water," J. Chem. Phys. **79**, 926–935 (1983).
[47]M. R. Shirts, "Simple quantitative tests to validate sampling from thermodynamic ensembles," J. Chem. Theory Comput. **9**, 909–926 (2013).
[48]P. T. Merz and M. R. Shirts, "Testing for physical validity in molecular simulations," PloS ONE **13**, e0202764 (2018).
[49]M. R. Shirts and J. D. Chodera, "Statistically optimal analysis of samples from multiple equilibrium states," J. Chem. Phys. **129**, 124105 (2008).
[50]P. V. Klimovich, M. R. Shirts, and D. L. Mobley, "Guidelines for the analysis of free energy calculations," J. Comput. Aided Mol. Des. **29**, 397–411 (2015).
[51]C. H. Bennett, "Efficient estimation of free energy differences from Monte Carlo data," J. Comput. Phys. **22**, 245–268 (1976).
[52]J. Wang, R. M. Wolf, J. W. Caldwell, P. A. Kollman, and D. A. Case, "Development and testing of a general amber force field," J. Comput. Chem. **25**, 1157–1174 (2004).
[53]C. I. Bayly, P. Cieplak, W. Cornell, and P. A. Kollman, "A well-behaved electrostatic potential based method using charge restraints for deriving atomic charges: the RESP model," J. Phys. Chem. **97**, 10269–10280 (1993).
[54]G. A. Tribello, M. Bonomi, D. Branduardi, C. Camilloni, and G. Bussi, "PLUMED 2: New feathers for an old bird," Comput. Phys. Commun. **185**, 604–613 (2014).
[55]J. Lemkul, "From proteins to perturbed Hamiltonians: A suite of tutorials for the GROMACS-2018 molecular simulation package [article v1. 0]," Living J. Comp. Mol. Sci. **1**, 5068 (2018).
[56]S. K. Kandasamy and R. G. Larson, "Molecular dynamics simulations of model trans-membrane peptides in lipid bilayers: a systematic investigation of hydrophobic mismatch," Biophys. J. **90**, 2326–2343 (2006).
[57]C. Oostenbrink, A. Villa, A. E. Mark, and W. F. Van Gunsteren, "A biomolecular force field based on the free enthalpy of hydration and solvation: the GROMOS force-field parameter sets 53A5 and 53A6," J. Comput. Chem. **25**, 1656–1676 (2004).
[58]O. Berger, O. Edholm, and F. Jähnig, "Molecular dynamics simulations of a fluid bilayer of dipalmitoylphosphatidylcholine at full hydration, constant pressure, and constant temperature," Biophys. J. **72**, 2002–2013 (1997).
[59]C. Kandt, W. L. Ash, and D. P. Tieleman, "Setting up and running molecular dynamics simulations of membrane proteins," Methods **41**, 475–488 (2007).
[60]H. J. Berendsen, J. P. Postma, W. F. van Gunsteren, and J. Hermans, "Interaction models for water in relation to protein hydration," in *Intermolecular forces* (Springer, 1981) pp. 331–342.
[61]S. Nosé, "A unified formulation of the constant temperature molecular dynamics methods," J. Chem. Phys. **81**, 511–519 (1984).
[62]H. Flyvbjerg and H. G. Petersen, "Error estimates on averages of correlated data," J. Chem. Phys. **91**, 461–466 (1989).
[63]W. L. Jorgensen and C. Jenson, "Temperature dependence of TIP3P, SPC, and TIP4P water from NPT Monte Carlo simulations: Seeking temperatures of maximum density," J. Comput. Chem. **19**, 1179–1186 (1998).
[64]T. Schneider, E. P. Stoll, and R. Morf, "Brownian motion of interacting and noninteracting particles subject to a periodic potential and driven by an external field," Phys. Rev. B **18**, 1417 (1978).
[65]G. Bussi and M. Parrinello, "Stochastic thermostats: comparison of local and global schemes," Comput. Phys. Commun. **179**, 26–29 (2008).
[66]S. C. Harvey, R. K.-Z. Tan, and T. E. Cheatham III, "The flying ice cube: velocity rescaling in molecular dynamics leads to violation of energy equipartition," J. Comput. Chem. **19**, 726–740 (1998).
[67]E. Rosta, N.-V. Buchete, and G. Hummer, "Thermostat artifacts in replica exchange molecular dynamics simulations," J. Chem. Theory Comput. **5**, 1393–1399 (2009).
[68]J. Wong-Ekkabut, M. S. Miettinen, C. Dias, and M. Karttunen, "Static charges cannot drive a continuous flow of water molecules through a carbon nanotube," Nat. Nanotechnol. **5**, 555–557 (2010).
[69]J. Wong-ekkabut and M. Karttunen, "The good, the bad and the user in soft matter simulations," Biochim. Biophys. Acta-Biomembranes **1858**, 2529–2538 (2016).
[70]S. M. J. Rogge, L. Vanduyfhuys, A. Ghysels, M. Waroquier, T. Verstraelen, G. Maurin, and V. Van Speybroeck, "A comparison of barostats for the mechanical characterization of metal–organic frameworks," J. Chem. Theory Comput. **11**, 5583–5597 (2015).
[71]T. Okabe, M. Kawata, Y. Okamoto, and M. Mikami, "Replica-exchange monte carlo method for the isobaric–isothermal ensemble," Chem. Phys. Lett. **335**, 435–439 (2001).
[72]T. Mori, J. Jung, and Y. Sugita, "Surface-tension replica-exchange molecular dynamics method for enhanced sampling of biological membrane systems," J. Chem. Theory Comput. **9**, 5629–5640 (2013).